Int. J. Electrochem. Sci., 16 **(2021)** Article Number: 21103, doi: 10.20964/2021.10.22

International Journal of
ELECTROCHEMICAL
SCIENCE
www.electrochemsci.org

Hexavalent Chromium Reduction at the Polypyrrole-Coated 304-Stainless-Steel-Electrode in a Filter-Press-Type Reactor

E.E. Villalobos-Neri[1], *U. Páramo-García*[1,*], *H. Hernández-Escoto*[2,*], *R. Mayen-Mondragon*[3], *N.V. Gallardo-Rivas*[1]

[1] Tecnológico Nacional de México/I. T. Cd. Madero, Centro de Investigación en Petroquímica, Prol. Bahía de Aldhair y Av. de las Bahías, Parque de la Pequeña y Mediana Industria, 89600, Altamira, Tamaulipas, MÉXICO
[2] Universidad de Guanajuato, Departamento de Ingeniería Química, Noria Alta s/n, 36050, Guanajuato, Gto., MÉXICO.
[3] Polo Universitario de Tecnología Avanzada, Facultad de Química, Universidad Nacional Autónoma de México, Vía de la Innovación 410, Autopista MTY-Aeropuerto Km. 10, Parque PIIT, 66629, Apodaca, Nuevo León, MÉXICO.
[*]E-mail: uparamo@itcm.edu.mx; hhee@ugto.mx

Received: 30 May 2021 / *Accepted:* 14 July 2021 / *Published:* 10 September 2021

In this work, the reduction of Cr(VI) to Cr (III) in a filter-press-type electrochemical-reactor is studied. The working electrode within the reactor is a polypyrrole-coated 304-stainless-steel plate. The polypyrrole was electropolimerized via 40 cyclic-voltammetry cycles. The deposit was characterized by Fourier Transform Infrared Spectroscopy, Optical Microscopy and Scanning Electron Microscopy. The Cr(VI)-ions solution was recirculated within the filter-press-type reactor and its concentration was monitored via the 1,5-diphenylcarbazide colorimetric technique. It was proposed that the Cr(VI)-removal process consists of a mechanism combining ion transport between the solution stream and the electrode, and reduction of Cr(VI) at the electrode. A mathematical model was then derived to describe the Cr(VI) evolution within the solution stream, and at the PPY electrode-layer. The model was validated with experimental data.

Keywords: conductive polymers, ion exchange, reduction, water contamination, mathematical model.

1. INTRODUCTION

Environmental pollution is one of the most important problems affecting our nowadays world. It has a direct impact on air quality, as well as the availability of water resources and agricultural soils. Both anthropogenic and natural contamination of waters by heavy metals is affecting food security and public health. For example, several studies have found heavy metals and metalloids in vegetables such

as lettuce, cabbage, squash, broccoli and potato due to irrigation with polluted water. In the same direction, toxic metals have also been found in fish, meat and milk as a result of bioaccumulation and mobility from the contamination point to adjacent water sources. Depending on the type of metal or metalloid, the toxicological effects in humans range from vital-organ damage to carcinogenic developments. Indeed, cases of health problems caused by the consumption of heavy-metal-contaminated food have been reported on a global level [1-3].

Chromium (Cr), like any transition metal, has several oxidation states. The most stable and frequent are trivalent chromium, Cr(III); and hexavalent chromium, Cr(VI), each one having significantly different chemical properties. Cr(VI) is considered the most toxic and carcinogenic form of chromium; it is found combined with oxygen as chromate or dichromate ions. In contrast, Cr(III), as an oxide, hydroxide or sulfate, is less mobile and can be found bound to organic matter in aquatic environments and soils. Cr(VI), being a strong oxidizing agent, is reduced to Cr(III) in the presence of organic matter [1,4-6]. However, high levels of Cr(VI) can overcome the reducing capacity of the environment and thus persist as pollutant. Cr(VI) poses a strong health risk to humans. Most affected are people working in the steel and textile industries. The chemical causes different health effects; when in contact with the skin, for example, it causes allergic reactions such as skin rashes, and when breathed, it can cause nose irritation and nosebleed. Other reported health problems are upset stomach and ulcers, respiratory problems, weakening of the immune system, kidney and liver damage, alteration of genetic material, lung cancer and death [5-8].

The recovery and removal of Cr(VI) species from water is needed in order to reduce its impact on human health and the environment. During the last decades, different remediation techniques such as those based in adsorption, chemical precipitation, membrane filtration and ion exchange were developed. Each of them, however, suffers from one or more drawbacks [2, 7, 8].

Electrochemical methods have application potential for water treatment, between them, the electrochemical-ion-exchange (EIE) process is of particular interest as, instead of chemical reagents, it uses an eco-friendly electric potential to promote ion exchange (IE). It has specific advantages over other methods such as longer EIE-resin life compared to the conventional ion exchange process, longer membrane life compared to the reverse osmosis/membrane filtration process, easier EIE-resin regeneration, output of target-contaminant-free water, and recovery of the target contaminant in pure form. Typical IE membranes used in the EIE process are made of conductive polymers with suitable catalytic properties towards the reduction of Cr(VI), as the Polyaniline, Polythiophene and Polypyrrole (PPY). Furthermore, they have application in organic batteries, electrochromic displays, chemical sensors, light emitting diodes, anticorrosive additives, among others [6-10].

Polypyrrole and its derived-compounds have recently gained much attention for the remediation of Cr(VI) ions in aqueous solutions. The material shows high electrical conductivity, non-toxicity, good environmental stability, low cost and ease of preparation. It is reported that the presence of a positively charged nitrogen atom within the PPY structure makes the material a suitable adsorbent of Cr(VI) ions in water. Furthermore, PPY facilitates the spontaneous reduction of toxic Cr(VI) into less toxic Cr(III) through a surface chemical reaction [8-14]. With all such considerations, the present work develops a mathematical model describing the combined EIE/reduction process of Cr(VI) to Cr(III) using a filter-press-type reactor and a 304-stainless-steel (AI-304) working-electrode coated

with an electrochemically-synthesized PPY-layer. The applied methodology and derived data can be useful to design new routes for the remediation of Cr(VI) present in water bodies.

2. EXPERIMENTAL

2.1. Polypyrrole-coating electrochemical synthesis and characterization

The PPY deposit, coating the perforated 304-stainless-steel plate (AI-304, geometric area 28 cm^2), was synthesized by electropolymerization via Cyclic Voltammetry with an Epsilon BASi Potentiostat. To that end, a conventional three-electrode-configuration cell was used with the perforated AI-304 as working electrode, an Ag/AgCl as reference electrode and the AI-304 plate as counter electrode. The electrolyte consisted of pyrrole (Aldrich, 99%) 0.1M and sulfuric acid (Aldrich, 99%) 0.1M [15-19]. The potential was scanned 40 times from -0.9 to 0.9 V vs. Ag/AgCl at 0.1 V/s. Prior to each experiment, the perforated plate was manually polished with 600-, 1200- and 1500-grit sandpaper until a smooth finish was achieved.

The chemical characterization of the PPY deposit was carried out by Fourier Transform Infrared Spectroscopy (FTIR) with a Perkin Elmer Spectrum 100, using the Attenuated Total Reflectance (ATR) module. Optical Microscopy (ODAR) and Scanning Electron Microscopy (JEOL JSM-6390LV) were used to analyze the deposit surface morphology [17-21].

2.2. Cr(VI) to Cr(III) reduction system

Figure 1 shows the sample-solution recirculation system used to perform the Cr(VI) to Cr(III) reduction. A plastic container (Figure 1a) holding 400 mL of the $K_2Cr_2O_7$ aqueous-solution (sample solution) is connected to a peristaltic pump (Figure 1b) which forces the sample solution to flow into the filter-press-type reactor (ElectroCell, Sweden). A power source (Figure 1c) is used then to apply -0.9 V of direct current (DC) to the AI-304 PPY-coated working-electrode within the reactor. The latter is done to promote the adsorption of Cr(VI) ions to the PPY layer and to reduce the oxidized PPY-active-sites after the Cr(VI) to Cr(III) reduction. The sample solution returns afterwards to the plastic container. Different initial $K_2Cr_2O_7$-concentrations were tested (50, 100 and 200 mg/L). The sample-solution pH was adjusted to 1 by adding sulfuric acid. The flow rate was set to 10 mL/min. All tests were conducted at room temperature. 1 mL aliquots of the sample-solution within the container were taken every 30 minutes during 4 h and sent to Cr(VI) analysis [20-28]. The Cr(VI) concentration was determined by the technique described in NOM-044. It is a colorimetric method employing 1,5 diphenylcarbazide to generate reddish-colored complexes with Cr(VI), which in turn can be then determined by Ultraviolet-Visible Spectroscopy at 540 nm. To this end, an Agilent Cary UV-Vis Spectrophotometer was used [26-32].

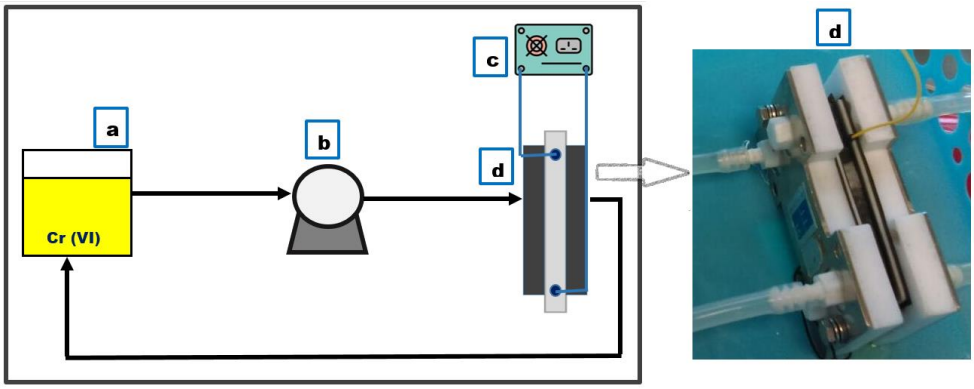

Figure 1. Recirculation system for the Cr(VI) to Cr(III) reduction, a) $K_2Cr_2O_7$ aqueous solution, b) peristaltic pump, c) power supply and d) filter-press type reactor.

2.3. Cr(VI) to Cr(III) reduction mathematical- model

2.3.1. Proposed reduction mechanism

The global reduction reaction of Cr(VI) to Cr(III) at the PPY layer is [33],

$$Cr_2O_7^{2-} + 6PPY^0 + 14H^+ \rightarrow 2Cr^{3+} + 6PPY^+ + 7H_2O \qquad \text{Eq. 1}$$

The Cr(VI) ions must first reach the PPY-layer on the reactor-working-electrode, where reduction to Cr(III) proceeds. The non-reduced Cr(VI)-ions-fraction together with the freshly-formed Cr(III) ions departs from the electrode surface. By considering the stream-regions formed within a liquid flowing along a plate [34], the Cr(VI) transport and reaction processes are proposed to be carried out as follows (depicted in Figure 2): 1) transport of exchangeable Cr(VI) ions within the sample solution flowing inside the reactor towards a boundary region close to the electrode, where the flow pattern becomes quasi-static, 2) transport of the Cr(VI) ions within the boundary layer towards the PPY-layer at the reactor-working-electrode, 3) ion exchange process through the reduction reaction (Eq. 1), 4) departure of non-reduced Cr(VI) ions away from the electrode surface through the boundary layer and 5) transport away of the boundary layer towards the sample-solution flowing inside the reactor [29-36].

2.3.2. Model construction

Considering the aforementioned mechanism, a quantitative description of the Cr(VI)-ions concentration within the different stream regions and at the working-electrode PPY-layer is constructed considering the following mass balances (Eq. 2),

$$\frac{dc_R}{dt} = -q_{RB} + q_{BR}, \quad \frac{dc_B}{dt} = q_{RB} - q_{BR} - q_{BE} + q_{EB}, \quad \frac{dc_E}{dt} = -r + q_{BE} - q_{EB}, \qquad \text{Eq. 2}$$

where c_R, c_B and c_E are the Cr(VI) concentrations in the sample-solution flowing inside the reactor, in the boundary-layer and at the electrode-PPY, respectively. The volume-normalized flow of Cr(VI) ions between the different stream regions (q_{RB}, q_{BR}), and between the boundary-layer and the electrode-PPY-layer (q_{BE}, q_{EB}) are considered in a convective-like form (Eq. 3),

$$q_{RB} = k_{RB}*(c_R - c_B),\ q_{BR} = k_{BR}*(c_B - c_R),\ q_{BE} = k_{BE}*(c_B - c_E),\ q_{EB} = k_{EB}*(c_E - c_B), \quad \text{Eq. 3}$$

where k_{RB}, k_{BR}, k_{BE} and k_{EB} are convective mass transfer constants. The Cr(VI) reduction is considered a first order reaction (Eq. 4),

$$r = k_r * c_E \quad \text{Eq. 4}$$

where k_r is the kinetic constant.

By combining the above expressions, the following mathematical model is obtained (Eq. 5 - 7):

$$\frac{dc_R}{dt} = -k_1 * (c_R - c_B), \qquad k_1 = k_{RB} - k_{BR}, \quad \text{Eq. 5}$$

$$\frac{dc_B}{dt} = k_1 * (c_R - c_B) - k_2 * (c_B - c_E), \qquad k_2 = k_{BE} - k_{EB}, \quad \text{Eq. 6}$$

$$\frac{dc_E}{dt} = -k_r * c_E + k_2 * (c_B - c_e) \quad \text{Eq. 7}$$

The model is a system of three first-order differential equations with a kinetic constant (k_r), and two convective mass-transfer constants (k_1 and k_2). These latter constants group those of the particular flows between stream regions. The structure of the model is linear, so an analytical solution can be obtained. However, a numerical method is resorted to for the sake of simulation practicality; in this case, the numerical solver called ODE23s of the Matlab® software was used.

2.3.3. Model identification

The parameters of the model were determined through a rough but effective technique that we called exhaustive search: the model was solved with every point (k_1, k_2, k_r) of a three-dimensional grilled space delimited by assumed minimum and maximum values of the model parameters; and for very run, a sum of the quadratic differences between the model prediction of c_R and the corresponding experimental value was calculated; the point (k_1^*, k_2^*, k_r^*) corresponding to the sum with the minimum value was then selected. It is worthy to mention that the numerical solution enabled this numerous runs evaluation and the required computation time was short, in order of minutes.

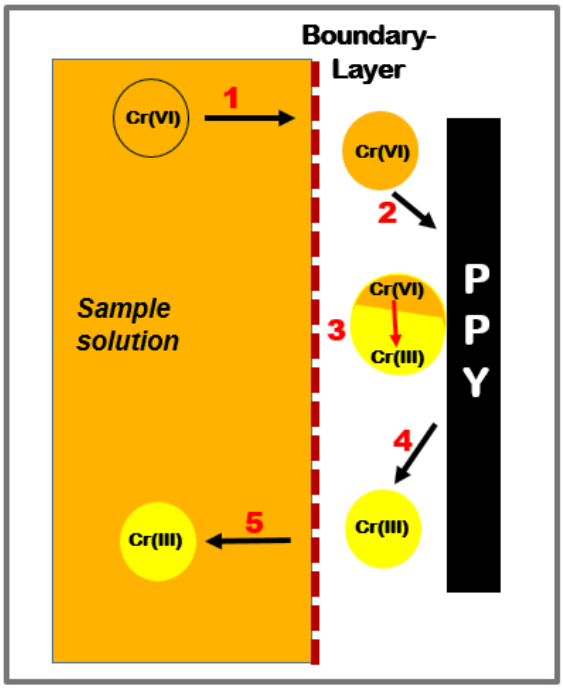

Figure 2. Stages of the Cr(VI) reduction mechanism: 1) transport of exchangeable Cr(VI) ions within the sample solution flowing inside the reactor towards the boundary region close to the electrode, 2) transport of the Cr(VI) ions within the boundary layer towards the PPY-layer at the reactor-working-electrode, 3) ion exchange process through the reduction reaction (Eq. 1), 4) departure of non-reduced Cr(VI) ions away from the electrode surface through the boundary layer and 5) transport away of the boundary layer towards the sample-solution flowing inside the reactor.

3. RESULTS AND DISCUSSION

3.1. Electrodeposit synthesis and characterization

Figure 3 shows the initial 10 voltammetric cycles acquired during the PPY-coating electrosynthesis procedure. PPY growth at the AI-304 surface takes place within potential range -0.8 to 0.8 V (Ag/AgCl). The first cycle indicates a sharp increase in the anodic current at about 0.65 V (Ag/AgCl) forming a large anodic oxidation peak of the monomer and thus polymer formation. The oxidation potential of the pyrrole shifted to more positive with the successive cycles due to the deposition of the polymer layers. The oxidation-reduction peaks of the polypyrrole are observed at 0.5/-0.7 V (Ag/AgCl). The area under the the charge/discharge region can be associated with the amount of deposited polymer [17-19, 26, 27, 34].

Figure 4 shows the FTIR spectrum of the synthesized PPY coating. The peaks at 813 cm^{-1}, 936 cm^{-1} are attributed to C–H wagging. The characteristic peaks at 1558.4 cm^{-1} and 1487 cm^{-1} correspond to the C=C stretching, whereas peaks at 1576 cm^{-1} and 1221 cm^{-1} represent to respectively, C=N and C–N bonds. The broad band observed at 3193 cm^{-1} is assigned to presence of N–H stretching vibrations. The peaks observed in the present work match well with the ones available in the literature

[19, 20, 35-38]. The observations confirm the deposit formed on the plate is PPY with some oxidation degree.

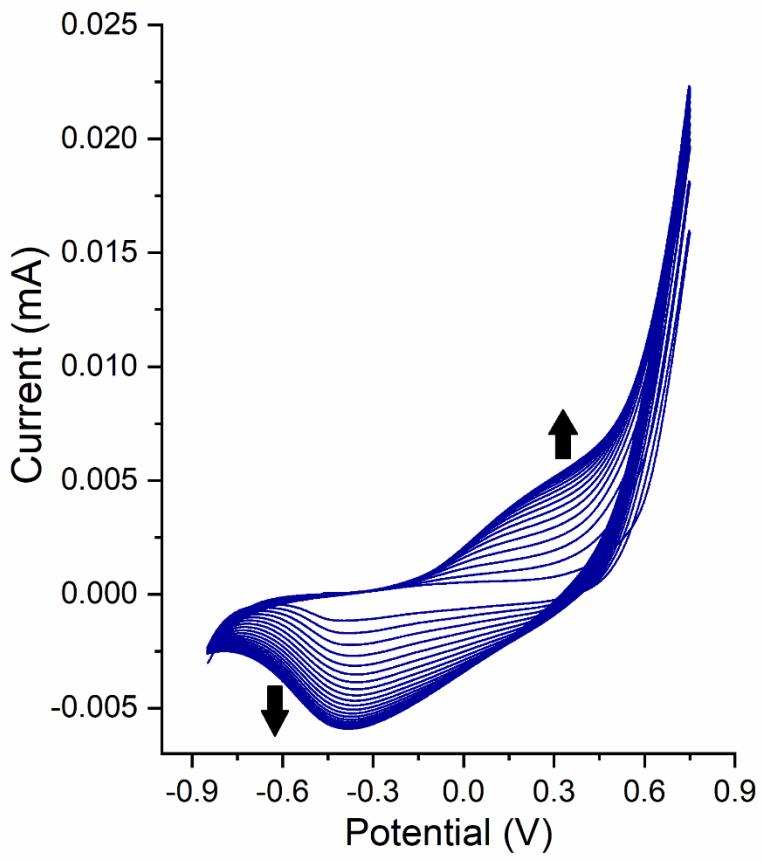

Figure 3. Initial 10 voltammetric cycles of the PPY electrosynthesis on top of a perforated 304-stainless-steel plate (working electrode) with an Ag/AgCl reference electrode and AI-304 plate as counter electrode. Electrolyte: Py 0.1M + H_2SO_4 0.1M. Scan rate 0.1 V/s.

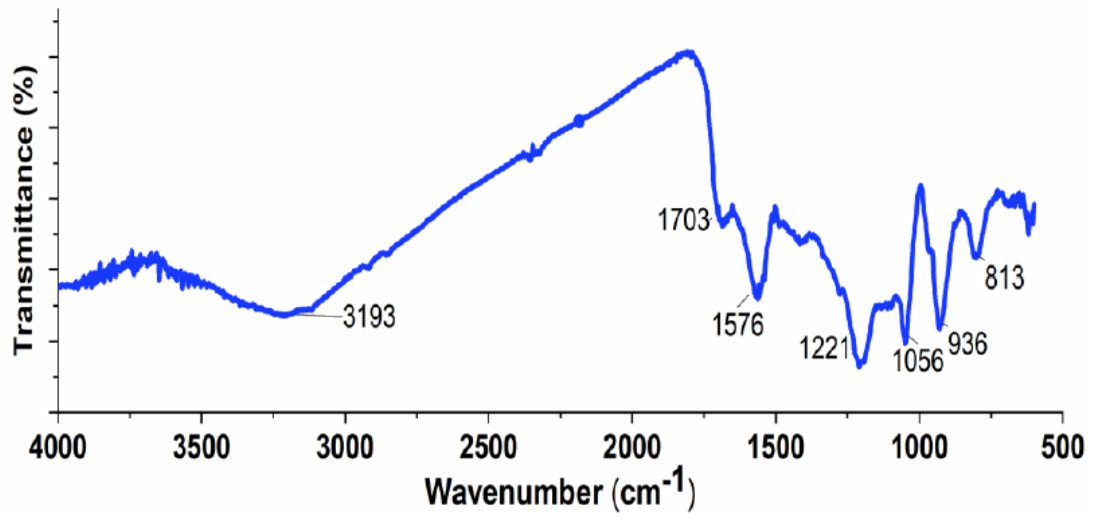

Figure 4. FTIR spectrum of the synthesized PPY coating over a AI-304 perforated steel plate.

Figure 5a shows an optical-microscopy-image of the AI-304 plate prior to the PPY deposit. Figure 5b shows the PPY-coating morphology, as observed under the microscope, at the end of the 40-voltammetric-cycles applied. An amorphous, apparently uniform and dark deposit is observed covering the steel substrate. Its structure is related to the selected electrosynthesis conditions [20, 37].

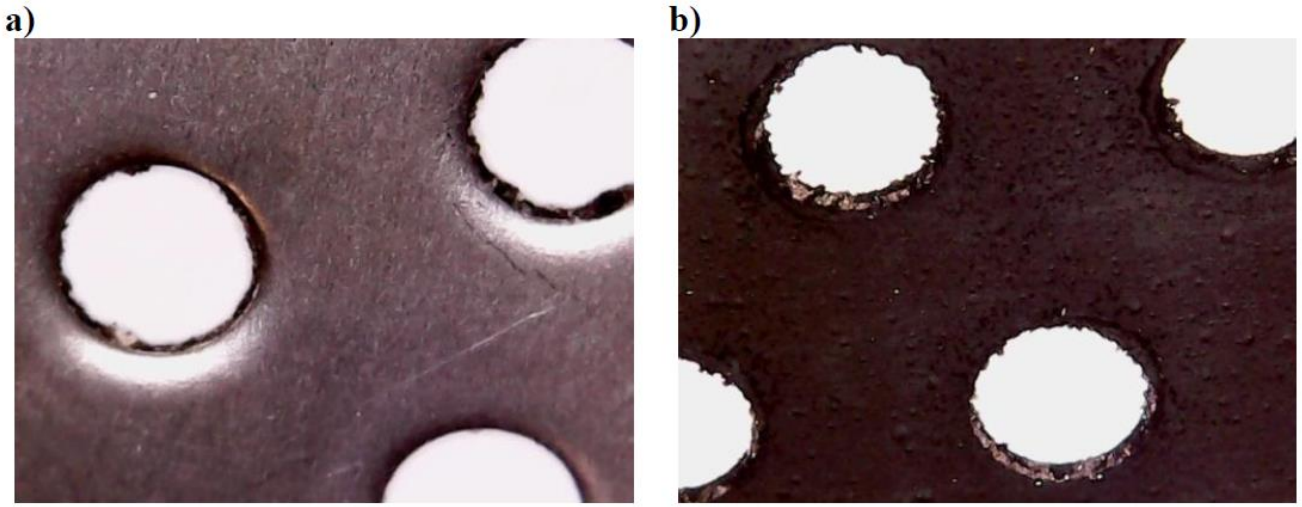

Figure 5. Optical microscopy images of a) AI-304 steel plate (substrate), b) PPY coating electrodeposit after the 40 voltammetric cycles applied

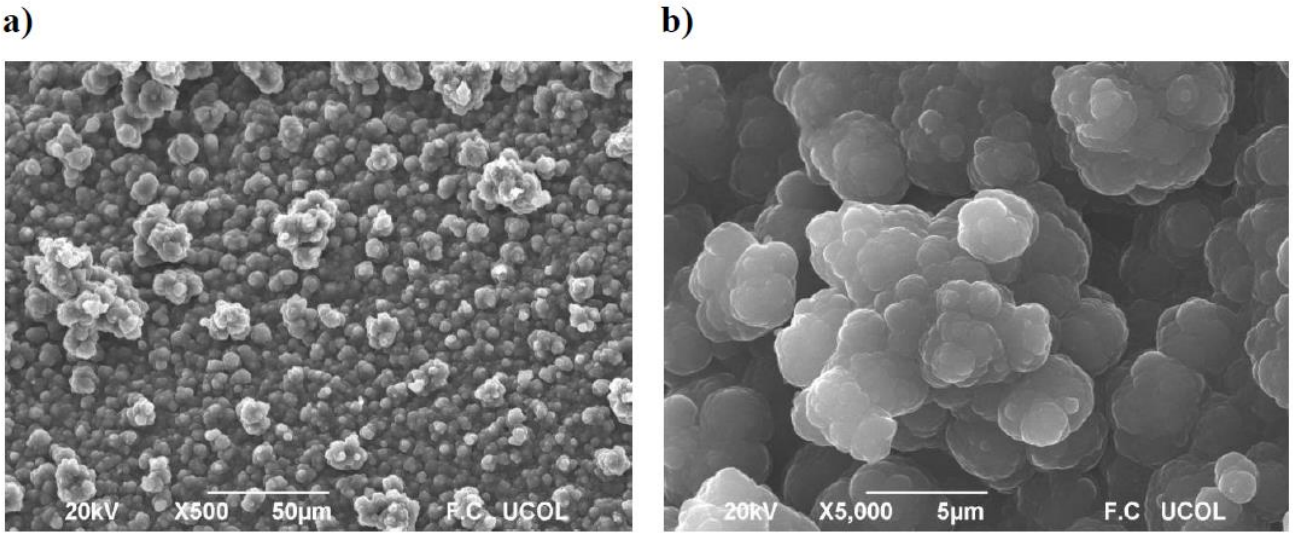

Figure 6. Scanning-electron-microscopy images of the PPY coating electrodeposit after the 40 voltammetric cycles applied.

3.2.1. Model Performance

The values of the model parameters were determined from a sequential use of outcomes of each experiment case corresponding to a particular Cr(VI) initial concentration; e.g., the c_R measurements as a function of time for the experiment with an initial Cr(VI) concentration of 50 mg/L were firstly used.

Each case consisted of three runs, so the model parameters were calculated for each run in order to verify reproducibility. After that, the three derived values of each parameter were averaged. The average values of each experiment case were compared to each other in order to verify they fell within the same order of magnitude. Table 1 shows the outcomes in k_1, k_2 and k_r. The values are consistent for the three different experiment cases studied.

Table 1. Values of model parameters determined from each experimental run.

Initial c_R (mg Cr(VI)/L)	k_1 (1/min)	k_2 (1/min)	k_r (1/min)	Average k_1	Average k_2	Average k_r
50	0.0091	0.77	0.86	0.00913	0.77333	0.87666
50	0.0091	0.77	0.86			
50	0.0092	0.78	0.88			
100	0.009	0.76	0.88	0.00903	0.76333	0.87666
100	0.0091	0.76	0.87			
100	0.009	0.77	0.88			
200	0.0092	0.76	0.88	0.00916	0.76333	0.87666
200	0.0092	0.76	0.87			
200	0.0091	0.77	0.88			

It is worthy to highlight that all the calculated values are positive. Thus, regarding the convective mass transfer constants k_1 and k_2, it means k_{RB} is larger than k_{BR}, and k_{BE} is larger than k_{EB}. In this way, the flow of Cr(VI) ions from within the sample solution to the boundary layer is greater than that in the reverse direction. The same applies for the flow between the boundary layer and the PPY layer. With respect to k_r, it confirms the reaction proceeds in the direction of Cr(VI) ion consumption.

Figure 7a compares the experimental data of each experiment case to the data predicted by the mathematical model. The simulated c_R continuous trajectory matches well the experimental c_R points. This describes a process in which the Cr(VI) initial concentration is gradually decreased to a low value within a time span of 240 min.

Figure 7b shows the model-estimated evolution of Cr(VI) concentration in the boundary layer (c_B), which is much lower than c_R. It can be confirmed that the values of the terms $k_1*(c_R - c_B)$ and $k_2*(c_B - c_E)$ in Eq. 2b, which are related to the ion-net-flow between the stream regions, are of the same magnitude order. At the start of the experiment, the first one is greater than the second one, leading to an accumulation of Cr(VI) ions in the boundary layer. However, the second one grows up fastly and matches the first one, halting the aforementioned Cr(VI) ion accumulation. Furthermore, the second term increases still so that the amount of ions leaving the boundary layer becomes greater than the one entering it, in such a way the Cr(VI) ion accumulation is diminished. This is reflected at the beginning of the c_B trajectory, where it fastly grows up to reach a maximum but then it starts to decrease. This behavior is observed in the c_E trajectory as well (Figure 7c); in this case, the term k_r*c_E

(Eq. 2c) compared to the term $k_2*(c_B - c_E)$ (Eq. 2c) is at first smaller, but it fastly grows up to become the largest one, resulting in a low amount of accumulated Cr(VI) ions [32-37, 41-54].

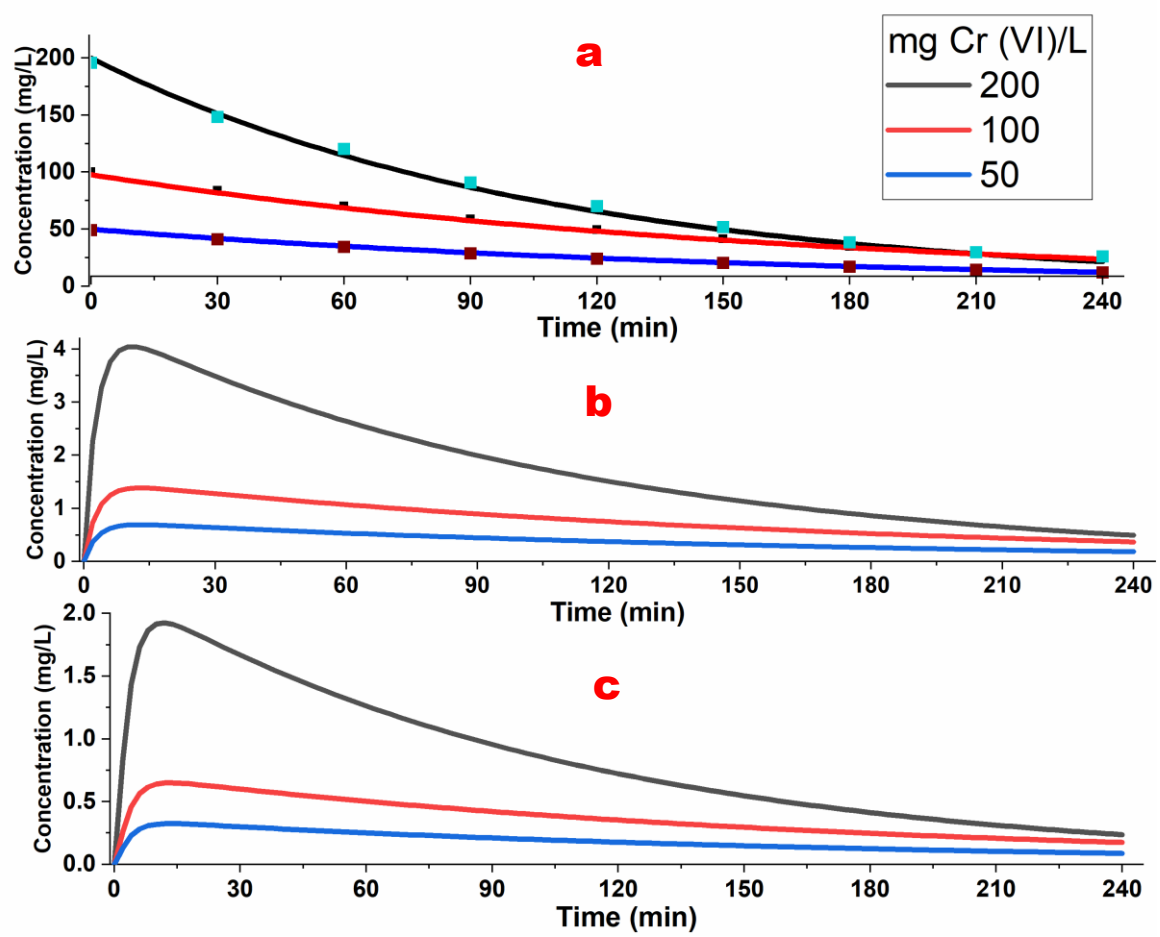

Figure 7. Model performance to describe the Cr(VI) concentration change (a) within the sample solution flowing inside the reactor, (b) in the boundary layer, and (c) at the electrode PPY-layer.

The good match between the simulated data generated by the model (Eqs. 5, 6, 7) and the experimental outcomes (Figure 7a) confirms the validity of the Cr(VI) reduction scheme depicted in Figure 2. It can be safely stated that the ion-transport step is the limiting step of the reduction process, since the term related to the net flow of ions from within the reactor stream to the boundary layer (Eq. 5 or Eq. 6) is of a lower order of magnitude, and the ions at the PPY layer are reduced at the rate at which they arrive to such layer. This results point to an advantage related to the PPY layer capacity: although the Cr(VI) concentration is relatively high within the sample solution flowing into the reactor, the PPY layer is only exposed to a low Cr(VI) concentration, thus its performance is not degraded by the high Cr(VI) concentration.

4. CONCLUSIONS

In this work, the Cr(VI) reduction process is carried out with a filter-press-type reactor whose working electrode is a PPY-coated stainless-steel plate. The reduction scheme was proposed to consist of a series of transport steps of Cr(VI) ions from the sample solution flowing into the reactor to the electrode, in addition to the Cr(VI) reduction reaction at the electrode. The mathematical model constructed on this basis, and validated with experimental outcomes, confirms the transport steps are the limiting step of the overall reduction process, and thus when the Cr(VI) ions reach the electrode layer, the Cr(VI) reduction reaction is fastly performed. In this way, the model can be taken as a basis for the interpretation and scaling-up of the Cr(VI) reduction process using electrodeposits with conductive polymers. From the application point of view, it would be interesting to find other possible uses of this type of electrochemical deposits as it is a broad and novel field of study.

ACKNOWLEDGMENTS
E.E. Villalobos-Neri acknowledges the scholarship provided by CONACYT-Mexico. The authors would like to thank Consejo Nacional de Ciencia y Tecnología (CONACYT-México) and Tecnológico Nacional de México (TecNM) for financial support (8123.20-P and 9268.20-P).

References

1. Y. Reyes, I. Vergara, O. Torres, M. D. Lagos and E. E. G. Jiménez. *Ing. Inv. Des*., 16 (2016) 66.
2. Y. Ma, W. J. Liu, N. Zhang, Y. S. Li, S. Jiang, and G. P. Sheng. *Bioresour. Technol*., 169 (2014) 403.
3. C. C. Kan, A. H. Ibe, K. K. P. Rivera, R. O. Arazo and M. D. G. Luna. *Sustainable Environ. Res*., 27 (2017) 163.
4. U. O. Aigbe and O. A. Osibote. *J. Environ. Chem. Eng*., (2020) 104503.
5. F. L. Long, C. G. Niu, N. Tang, H. Guo, W. W. Li, Y. Y. Yang and L. S. Lin. *Chem. Eng. J*., 404 (2021) 127084.
6. N. S. Alsaiari, A. Amari, K. M. Katubi, F. M. Alzahrani, F. B. Rebah and M. A. Tahoon. *Processes*, 9 (2021) 576.
7. N. H. Kera, M. Bhaumik, K. Pillay, S. S. Ray and A. Maity. *Mater. Today Commun*., 15 (2018) 1534.
8. R. Karthik and S. Meenakshi. *Desalin. Water Treat*., 56 (2015) 1587.
9. Y. Tian, L. Huang, X. Zhou and C. Wu. *J. Hazard. Mater*., 225 (2012) 15.
10. S. M. Riahi, S. M. Borghei, A. Olad and M. J. Chaichi. *Iran. J. Chem. Chem. Eng.*, 30 (2011) 97.
11. M. R. Samani and D. Toghraie. *Journal of Environmental Health Science and Engineering*, 17 (2019) 53.
12. Y. Zhan, S. He, X. Wan, J. Zhang, B. Liu, J. Wang, Z. Li. J. *Colloid Interface Sci*., 529 (2018) 385.
13. J. Wang, K. Pan, Q. He and B. Cao. *J. Hazard. Mater*., 244 (2013) 121.
14. U. Baig, R. A. K. Rao, A. A. Khan, M. M. Sanagi and M. A. Gondal. *Chem. Eng. J.*, 280 (2015) 494.
15. L. Du, P. Gao, Y. Liu, T. Minami and C. Yu. *Nanomater.*, 10 (2020) 686.
16. M. Janmohammadi, M. Baghdadi, T. M. Adyel, and N. Mehrdadi. *Sci. Total Environ*., 752 (2021) 141850.
17. Z. A. Chaleshtari and R. Foudazi. *ACS Appl. Polym. Mater*., 2 (2020) 3196-3204.
18. M. Li, J. Zhou, Y. G. Bi, S. Q. Zhou and C. H. Mo. *Sep. Purif. Technol*., 256 (2021) 117805.
19. A. Hosseinkhani, B. F. Rad and M. Baghdadi. *J. Environ. Manage*., 274 (2020) 111153.

20. L. Du, P. Gao, Y. Meng, Y. Liu, S. Le, and C. Yu. *ACS Omega*, 5 (2020) 6651.
21. V. E. Pakade, N. T. Tavengwa and L. M. Madikizela. *RSC Adv*., 9 (2019) 26142.
22. M. R. Gandhi, N. Viswanathan and S. Meenakshi. *Ion Exch. Lett*., 3 (2010) 25.
23. S. Plummer, C. Gorman, T. Henrie, K. Shimabuku, R. Thompson, and C. Seidel. *Water Res*., 139 (2018) 420.
24. M. K. Dinker and P. S. Kulkarni. *J. Chem. Eng. Data*, 60 (2015) 2521.
25. B. Qiu, C. Xu, D. Sun, Q. Wang, H. Gu, X. Zhang and S. Wei. *Appl. Surf. Sci*., 334 (2015) 7.
26. W. Duan, G. Chen, C. Chen, R. Sanghvi, A. Iddya, S. Walker and D. Jassby. *J. Membr. Sci*., 531 (2017) 160.
27. M. Bhaumik, A. Maity, V. V. Srinivasu, and M. S. Onyango. *Chem. Eng. J.*, 181 (2012) 323.
28. S. Wang, H. L. Ma, J. Peng, Y. Zhang, J. Chen, L. Wang and M. Zhai. *Dalton Trans*., 44 (2015) 7618.
29. K. Mukherjee, R. Saha, A. Ghosh, and B. Saha. *Res. Chem. Intermed*., 39 (2013) 2267.
30. L. Alvarado, I. R. Torres and A. Chen. *Sep. Purif. Technol*., 105 (2013) 55.
31. S. P. Paredes-Carrera, R. F. Valencia-Martínez, M. A. Valenzuela-Zapata, J. C. Sánchez-Ochoa and L. V. Castro-Sotelo. *Rev. Mex. Ing. Chim*., 14 (2015) 429-436.
32. A. F. C. Campos, H. A. L de Oliveira, F. N. da Silva, F. G. da Silva, P. Coppola, R. Aquino and J. Depeyrot. *J. Hazard. Mat*., 362 (2019) 82.
33. Y. Tian, L. Huang, X. Zhou, and C. Wu. *J. Hazard. Mat*., 225 (2012) 15.
34. R. B. Bird, W. E. Stewart and E. N. Lightfoot, Transport Phenomena, Revised 2nd Edition, Wiley (2006).
35. U. K. Garg, M. P. Kaur, V. K. Garg, and D. Sud. *J. Hazard. Mat*., 140 (2007) 60.
36. K. K. Krishnani, S. Srinives, B. C. Mohapatra, V. M. Boddu, J. Hao, X. Meng and A. Mulchandani. *J. Hazard. Mat*., 252 (2013) 99.
37. H. Zhang, Y. Tang, D. Cai, X. Liu, X. Wang, Q. Huang and Z. Yu. *J. Hazard. Mat*., 181 (2010) 801.
38. H. Wang, X. Song, H. Zhang, P. Tan and F. Kong. *J. Hazard. Mat*., 384 (2020) 121459.
39. M. Owlad, M. K. Aroua, W. A. W. Daud and S. Baroutian. *Water, Air, and Soil Pollution*, 200 (2009) 59.
40. J. A. Korak, R. Huggins and M. Arias-Paic. *Water research*, 118 (2017) 141.
41. J. Zhao, Z. Li, J. Wang, Q. Li and X. Wang. *J. Mat. Chem*. A, 3 (2015) 15124.
42. D. Park, Y. S. Yun, J. H. Jo, and J. M. Park. *Water Res*., 39 (2005) 533.
43. C. Bengoa, A. Montillet, P. Legentilhomme and J. Legrand, *J. Appl. Electrochem*., 27 (1997) 1313.
44. E. Pehlivan and H. T. Kahraman. *Food Chem*., 133 (2012) 1478.
45. G. Beretta, M. Daghio, A. Espinoza-Tofalos, A. Franzetti, A. F. Mastorgio, S. Saponaro and E. Sezenna. *Water*, 12 (2020) 466.
46. M. Griffiths, C. P. de León and F. C. Walsh. *AIChE J*., 51 (2005) 682.
47. F. F. Rivera, C. P. de León, F. C. Walsh and J. L. Nava. *Electrochim. Acta*, 161 (2015) 436.
48. J. Guzmán, J. G. Ibañez, R. C. Vásquez and M. T. Oropeza. *Bull. Electrochem*. 20 (2004) 107.
49. F. F. Rivera, C. P. de León, J. L. Nava and F. C. Walsh. *Electrochim. Acta*, 163 (2015) 338.
50. L. Rafati, A. H. Mahvi, A. R. Asgari and S. S. Hosseini. *Int. J. Environ. Sci. Technol*., 7 (2010) 147.
51. S. Rengaraj, C. K. Joo, Y. Kim and J. Yi, *J. Hazard. Mat*., 102 (2003) 257.
52. M. S. Bhatti, A. S. Reddy, R. K. Kalia and A. K. Thukral. *Desalin.*, 269 (2011) 157.
53. L. A. M. Ruotolo and J. C. Gubulin. *React. Functi. Polym*., 62 (2005) 141.
54. A. S. Dharnaik and P. K. Ghosh. *Environ. Technol*., 35 (2014) 2272.